Trans. Phenom. Nano Micro Scales, 2(1): 29-42, Winter - Spring 2014
DOI: 10.7508/tpnms.2014.01.003

ORIGINAL RESEARCH PAPER

Numerical Study of Hydro-Magnetic Nanofluid Mixed Convection in a Square Lid-Driven Cavity Heated From Top and Cooled From Bottom

A. Zare Ghadi [1], M. Sadegh Valipour [1,*]
[1]*Mechanical Engineering Department, University of Semnan ,Semnan, I.R. Iran*

ARTICLE INFO.

Article history
Received 21 April 2013
Accepted 29 November 2013

Keywords
Lid-Driven Cavity
MHD Flow
Mixed Convection
Nanofluid,

Abstract

In the present research mixed convection flow through a copper-water nanofluid in a driven cavity in the presence of magnetic field is investigated numerically. The cavity is heated from top and cooled from bottom while its two vertical walls are insulated. The governing equations including continuity, N-S and energy equations are solved over a staggered grid system. The study is conducted for Grashof number10^3 to 10^5, Hartmann number 0 to 100 and volume fraction number 0 to 5% while Reynolds number is fixed at 100. Hamilton–Crosser and Brinkman models have estimated effective thermal conductivity and effective viscosity of nanofluid, respectively. It is observed that magnetic field has unconstructive effect on heat transfer process whereas nanoparticles increase heat transfer rate.

1. Introduction

The prediction of fluid flow and heat transfer in a lid-driven cavity have been investigated through the past decades, because of its significance in many engineering applications such as building applications, solar collectors, nuclear reactors and crystal growth. In the latter case, fluid experiences magnetic field. There are some studies about mixed convection in lid-driven cavity under the effect of magnetic field. To review researches related to our study, we divide them into three categories:
1-Mixed convection in lid-driven enclosures with various boundary conditions.
2-Magnetic effect on mixed convection in lid- driven enclosures
3-Mixed convection in lid-driven enclosures using nanofluid.

1- There have been numerous studies in the past on mixed convection in lid-driven enclosures. Oztop and Dagtekin [1] discussed on mixed convection in a two-sided lid-driven differentially heated cavity. It is found that both Richardson number and direction of moving walls affect the fluid flow and heat transfer in the cavity. Sharif [2] studied the mixed convection in a shallow inclined driven cavity for various Richardson numbers. He indicated that the average convection in deep lid-driven cavities heated from below. They observed that the heat transfer was rather insensitive to the Richardson number.
2- There are limited studies on effects of MHD mixed convection in lid-driven cavities. Rahman et al. [7] numerically studied the MHD combined convection flow in an obstructed driven cavity under the effect of Joule heating. Their numerical results indicated that the Hartmann number, Reynolds number and Richardson number have strong influence on the

*Corresponding author:
Email address:msvalipour@semnan.ac.ir

streamlines and isotherms. They also deduced Joule heating parameter has little effect on the streamline and isotherm plots. Chamkha [8] reported a numerical investigation on hydromagnetic combined convection flow in a lid-driven cavity with internal heat generation or absorption.

The presence of the internal heat generation effects was found to decrease the average Nusselt number considerably for aiding flow and to increase it for opposing flow. Sivasankaran et al. [9] numerically studied the Hydro-magnetic mixed convection in a cavity with sinusoidal boundary conditions at the sidewalls. They indicated that the flow behavior and heat transfer rate inside the cavity are.

Nomenclature

B_0	Magnetic flux density ($wb.m^{-2}$)	α	Thermal diffusivity (m^2s^{-1}),($=K/\rho c_p$)
Gr	Grashof number($=g\beta\Delta TH^3.\nu_f^{-2}$)	β	Coefficient of volume expansion (s^{-1})
Ha	Hartmann number($=B_0H\sqrt{\sigma_f/\mu_f}$)	κ	Thermal conductivity ($W.(mK^{-1})$)
Nu	Local Nusselt number	φ	Solid volume fraction
Nu_{ave}	Average Nusselt number	μ	Dynamic viscosity ($Ns.m^{-2}$)
p	Non dimensional Pressure	ν	Kinematic viscosity ($m.^2s^{-1}$), ($=\mu.\rho^{-1}$)
Pr	Prandtel number($=v_f.\alpha_f$)	θ	Dimensionless coordinate
Re	Reynolds number($=\rho_f U_0 H/\mu_f$)	ρ	Density ($kg.m^{-3}$)
T	Fluid temperature (K)	σ	Electrical conductivity ($\Omega^{-1}m^{-1}$)
T_C	Temperature of cold wall (K)	ψ	Stream function
T_H	Temperature of hot wall (K)		**Subscripts**
u,v	Dimensional velocities ($m.s^{-1}$)	∞	Free stream
U,V	Dimensionless velocities	s	Solid
U_0	Top lid velocity ($m.s^{-1}$)	w	Wall
x, y	Dimensional coordinate	nf	Nanofluid
X, Y	Dimensionless coordinate	f	Fluid

strongly affected by the presence of the magnetic field. Oztop et al. [10] investigated MHD mixed convection in a lid-driven cavity with corner heater with various lengths. They showed that the heater length has significant effect on flow regime and heat transfer. They also concluded that an increase in Hartmann number leads to a decrease in flow strength and heat transfer rate.

3- There are some studies on effects of nanoparticles on mixed convetion in a lid-driven cavity. Tiwari and Das [11] made a work on heat transfer in a two-slided lid-driven enclosure using nanofluids; the left and the right wall are maintained at different constant temperatures while the upper and the bottom walls are thermally insulated. They illustrated that nanoparticles embedded in fluid are capable of increasing the heat transfer capacity of base fluid. They also indicated the variation of average Nusselt number is nonlinear with solid volume fraction. Talebi et al. [12] numerically studied mixed convection flow in lid-driven cavity using copper-water nanofluid. In their work, the top and bottom horizontal walls are insulated while the vertical walls are maintained at constant but different temperatures. It is observed that at the fixed Reynolds number, the solid concentration affects on the flow pattern and thermal behavior particularly for a higher

Rayleigh number. Abu-Nada and Chamkha [13] investigated combined convection in a tilted lid-driven cavity filled with a nanofluid. It is found that significant heat transfer enhancement can be obtained due to the presence of nanoparticles and that this is accentuated by inclination of the enclosure at moderate and large Richardson numbers.

As discussed above, magnetic field decreases heat transfer rate whereas nanoparticles immersed in base fluid increase it. Therefore, in such engineering applications where fluid is inevitably subjected to magnetic field; performance of heat and fluid flow is augmented by adding nanoparticles in base fluid. This novel idea has been scarcely studied in the literature. Hamad et al. [14] reported magnetic field effect on nanofluid flow past a vertical plate. Later on Hamad [15] analytically investigated on natural convection of nanofluid flow for a sheet in the presence of magnetic field. Recently, Ghasemi et al. [16] analyzed natural convection in a nanofluid-filled cavity in the presence of magnetic field. Their results showed that the heat transfer rate increases with an increase of the Rayleigh number but it decreases with an increase of the Hartmann number.

The main motivation of this work is to study the effects of magnetic field on mixed convection flow in a lid-driven cavity filled with copper-water nanofluid. As mentioned before two horizontal walls of cavity are at constant but different temperature, as top moving wall is hot and bottom wall is cold. Left- and right-hand sidewalls are thermally insulated.

2. Mathematical modeling

2.1. Governing equations

Fig. 1 shows a schematic configuration of the computational domain and coordinate systems used in the present study.

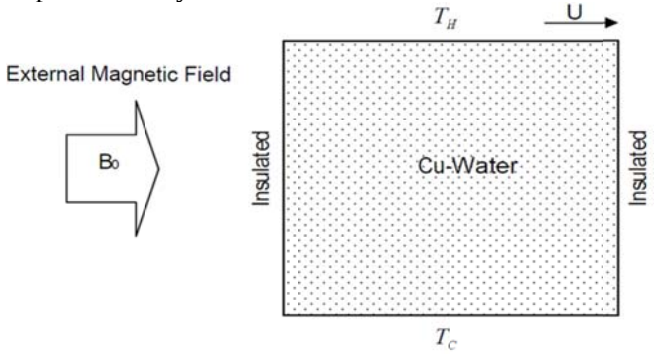

Fig. 1. Schematic of computational domain and coordinate system

It is presumed that the flow is steady, laminar, incompressible and single-phase model is considered for copper-water nanofluid. With neglecting induced magnetic field and assuming electrical field to be zero the Lorentz force can be simplified as . Dimensional equations are as follows.

Continuity

$$\frac{\partial u}{\partial x}+\frac{\partial v}{\partial y}=0 \tag{1}$$

x-Momentum equation

$$\left(u\frac{\partial u}{\partial x}+v\frac{\partial u}{\partial y}\right)=-\frac{1}{\rho_{nf}}\frac{\partial p}{\partial x}+\nu_{nf}\left(\frac{\partial^2 u}{\partial x^2}+\frac{\partial^2 u}{\partial y^2}\right) \tag{2}$$

y-Momentum equation

$$\begin{aligned}\left(u\frac{\partial v}{\partial x}+v\frac{\partial v}{\partial y}\right)&=-\frac{1}{\rho_{nf}}\frac{\partial p}{\partial y}+\nu_{nf}\left(\frac{\partial^2 v}{\partial x^2}+\frac{\partial^2 v}{\partial y^2}\right)\\&+\frac{g}{\rho_{nf}}(T-T_\infty)\left[\varphi\rho_s\beta_s+(1-\varphi)\rho_f\beta_f\right]-\frac{\sigma_{nf}B_0^2}{\rho_{nf}}\end{aligned} \tag{3}$$

Energy Equation:

$$\left(u\frac{\partial T}{\partial x}+v\frac{\partial T}{\partial y}\right)=\alpha_{nf}\left(\frac{\partial^2 T}{\partial x^2}+\frac{\partial^2 T}{\partial y^2}\right) \tag{4}$$

Eqs. (1)-(4) can be rewritten in the dimensionless forms by definition of the following parameters:

$$\begin{aligned}&X=\frac{x}{H},\ Y=\frac{y}{H},\ U=\frac{u}{U_0},\ V=\frac{v}{U_0}\\&\theta=\frac{T-T_C}{T_H-T_C},\ P=\frac{p}{\rho_{nf}U_0{}^2},\ \mathrm{Re}=\frac{\rho_f U_0 H}{\mu_f}\\&\mathrm{Pr}=\frac{\nu_f}{\alpha_f},\ Gr=\frac{g\beta\Delta TH^3}{\nu_f^2},\ Ha=B_0H\sqrt{\frac{\sigma_f}{\mu_f}}\end{aligned} \tag{5}$$

Therefore, dimensionless forms of the governing equations (Eqs. 1- 4) may be expressed as the following:

Continuity

$$\frac{\partial U}{\partial X}+\frac{\partial V}{\partial Y}=0 \tag{6}$$

X-Momentum equation

$$\left(U\frac{\partial U}{\partial X}+V\frac{\partial U}{\partial Y}\right)=-\frac{\partial P}{\partial X}+\frac{1}{\mathrm{Re}}\frac{\rho_f}{\rho_{nf}}(1-\varphi)^{-2.5}\left(\frac{\partial^2 U}{\partial X^2}+\frac{\partial^2 U}{\partial Y^2}\right) \tag{7}$$

Y- Momentum equation

$$\left(U\frac{\partial V}{\partial X}+V\frac{\partial V}{\partial Y}\right)=-\frac{\partial P}{\partial Y}+\frac{1}{\mathrm{Re}}\frac{\rho_f}{\rho_{nf}}\left((1-\varphi)^{-2.5}\left(\frac{\partial^2 V}{\partial X^2}+\frac{\partial^2 V}{\partial Y^2}\right)-(1+3\varphi)Ha^2V\right)+\frac{Gr}{\mathrm{Re}^2}\frac{\rho_f}{\rho_{nf}}\left(1-\varphi+\varphi\frac{\rho_s\beta_s}{\rho_f\beta_f}\right)\theta \tag{8}$$

Energy equation

$$U\frac{\partial \theta}{\partial X}+V\frac{\partial \theta}{\partial Y}\Big)=\frac{k_{nf}}{k}\frac{(\rho c_p)_f}{(\rho c_p)_{nf}}\frac{1}{\mathrm{Re}\,\mathrm{Pr}}\left(\frac{\partial^2\theta}{\partial X^2}+\frac{\partial^2\theta}{\partial Y^2}\right) \tag{9}$$

2.2 Thermo- physical properties of nanofluid

The electrical conductivity is as below (Maxwell's model) [17]:

$$\sigma_{nf}=(1+3\varphi)\sigma_f \quad (\text{Where } \sigma_s >> \sigma_f) \tag{10}$$

The viscosity of nanofluid is approximated by Brinkman [18] as the following:

$$\mu_{nf}=\frac{\mu_f}{(1-\varphi)^{2.5}} \tag{11}$$

The density of the nanofluid is estimated as the follows:

$$\rho_{nf}=(1-\varphi)\rho_f+\varphi\rho_s \tag{12}$$

The heat capacitance of nanofluid is expressed as the follows:

$$(\rho c_p)_{nf}=(1-\varphi)(\rho c_p)_f+(\varphi\rho c_p)_s \tag{13}$$

The effective thermal conductivity of the nanofluid is approximated by the model given by Patel et al. [19] as the following:

$$\frac{\kappa_{nf}}{\kappa_f}=1+\frac{k_s A_s}{k_f A_f}+ck_s Pe\,\frac{A_s}{k_f A_f} \tag{14}$$

Where c is constant and must be determined experimentally (for this study$c=3.6\times10^4$), A_s/A_f and Pe are defined as:

$$\frac{A_s}{A_f}=\frac{d_f}{d_s}\frac{\varphi}{1-\varphi},\ Pe=\frac{u_s d_s}{\alpha_f} \tag{15}$$

With d_s is the diameter of the solid particles that in this study is presumed to be equal to 100 nm,d_f is molecular size of liquid that is taken as 2Å for water. Also u_s is the Brownian motion velocity of nanoparticles which is defined as

$$u_s=\frac{2k_bT}{\pi\mu_f d_s^2} \tag{16}$$

Where k_b is the Boltzmann constant.

Table 1
presents thermo-physical properties of water and copper at the reference temperature.

Property	Water	Copper
c_p	4179	383
ρ	997	8954
κ	0.6	400
β	2.1×10^{-4}	1.67×10^{-5}

2.3. Boundary Conditions

According to Fig. 1 the governing equations (1)-(4) are subjected to the following boundary conditions:

Top wall

$$(0 \le X \le 1 \quad @ \quad Y = 1)$$
$$U = 1 \ , \ V = 0 \ , \ \theta = 1 \tag{17}$$

Bottom wall

$$(0 \le X \le 1 \quad @ \quad Y = 0)$$
$$U = V = 0 \ , \ \theta = 0 \tag{18}$$

Left and right walls :

$$(0 \le Y \le 1 \quad @ \quad X = 0 \ \& \ 1)$$
$$U = V = 0 \ , \ \frac{\partial \theta}{\partial x} = 0 \tag{19}$$

2.4. Auxiliary equations

When the velocity and temperature fields are calculated, the relations described by the following are applied to estimate local and average .The local Nusselt number is evaluated at the wall of the cavity as follows:

$$Nu = -\frac{k_{nf}}{k_f}\left(\frac{\partial \theta}{\partial Y}\right)_{Y=1} \tag{20}$$

The surface averaged value of Nusselt number on the cavity wall is calculated by the following relation:

$$Nu_{ave} = \int_0^1 Nu dX \tag{21}$$

3. Numerical solution

3.1. Solution technique

The governing equations mentioned in previous section are solved with algorithm SIMPLE (semi-implicit method for pressure-linked equations) introduced by Patankar [20]. This algorithm was successfully implemented for many problems of newtonian fluid flow and heat transfer in both laminar and turbulent situations. Central difference scheme is used to discretize the diffusion terms whereas a combination of upwind and central difference is adopted for discretizing the convection terms. The resulting discretized equations are solved iteratively by Tri-diagonal matrix algorithm (TDMA) [21]. Te iteration process is terminated when the following condition is satisfied

$$\left|\frac{\sum\left(\phi_{i,j}^{t} - \phi_{i,j}^{t-1}\right)}{\sum \phi_{i,j}^{t}}\right| \le 10^{-6} \tag{22}$$

Where Φ refers to θ, U ,V and t indicates the iteration step.

3.2. Grid independence study

To study the grid independence examination, the numerical procedure is carried out for different grid resolutions. The grids sensitivity analysis is performed for Re=100 ,Gr=10^3, $\varphi = 0.05$ and Ha=0 .Table 2 indicates the impact of the number of grid points on the average Nusselt number on the top wall of the cavity. According to percentage difference of different grids in last column the uniform grid system of 81× 81 is fine enough to attain accurate outcome in this work.

Table 2

Effect of grid number on Nu_{ave} at $\mathrm{Re} = 100$, $\mathrm{Pr} = 6.2$, $Gr = 10^3$, $\varphi = 0.05$ and $Ha = 0$

Number of Grids	Nu_{ave}	Percentage difference
21 × 21	4.8515	
		1.03 %
41 × 41	4.8017	
		0.64 %
61 × 61	4.7709	
		0.15 %
81 × 81	4.7637	
		0.07 %
101 × 101	4.7601	

3.3. Validation

In order to validate our numerical solution, calculated local Nusselt number in top hot wall and U velocity in centerline of enclosure are compared with

those of Iwatsu et al [4]. As it is shown in Fig. 2, the local Nusselt number and u velocity are found to be in good agreement comparing with the results of Iwatsu et al [4].

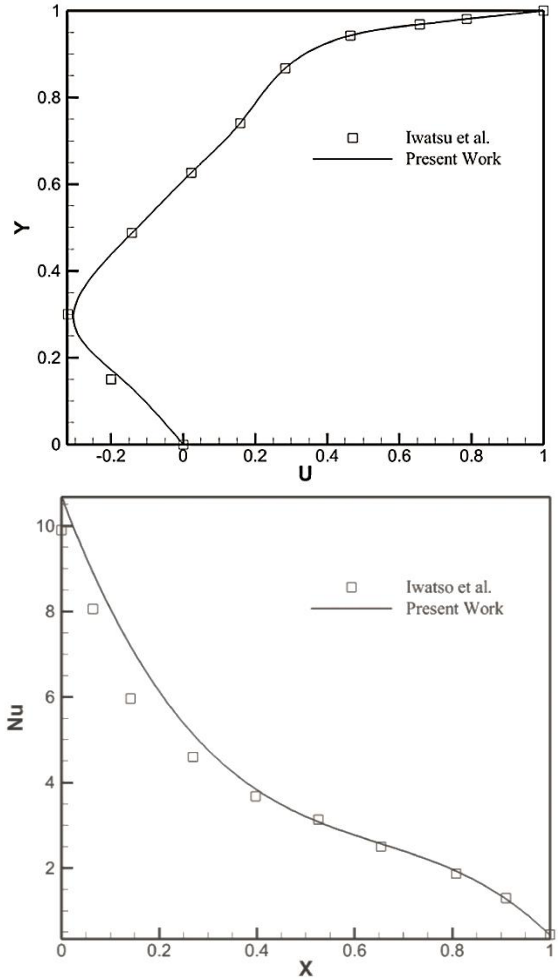

Fig. 2. Comparison of a) the U-profile at the middle of enclosure and b) the Nusselt number at the top wall at Re=400 & Gr=10^6

4. RESULTS AND DISCUSSIONS

The streamlines for various Grashof numbers and Hartmann numbers are shown in Fig. 1; The solid and dashed lines are corresponded to clear fluid and nanofluid ($\varphi = 0.05$), respectively. As can be seen in Fig 3 the effect of lid-driven flow is dominant for $G_r = 10^3$ in the absence of the magnetic field; The main circulation covers the entire cavity and two minor bubbles are formed near the bottom corners. Because the magnetic field has the inclination to decelerate the working fluid in the cavity, when the Hartmann number is increased, the main circulation inhibits progressively and secondary bubble is formed at the bottom of cavity. When the Hartmann number is increased from 30 to 100 the primary and secondary circulations in the flow are gradually limited to the area at the top and middle of the cavity and the flow near the bottom of cavity becomes almost stagnant. Increase in Grashof number to 10^4 augments the buoyancy effect; but the effect of the force convection is still observed. When Grashof number is increased to 10^5 prominent buoyancy-driven convective characteristics are noticeable and much of the middle and bottom parts of working fluid is stagnant. In this case the augmentation of magnetic field from 30 to 100 does not have substantial effect on the flow pattern because the flow is stagnant in the bulk of the cavity. Fig. 3 also indicates that the strength of circulations increases by increasing solid volume fraction for lower Grashof number, whereas it remains almost unchanged for higher Grashof number.

The temperature contours are depicted in Fig. 4 for different Gr and Ha numbers for both clear fluid and nanofluid. Where dashed lines are used for nanofluid and solid lines are used for clear fluid. For Grashof number 10^3 and in the absence of the magnetic field temperature distribution is steep near the bottom of the cavity. In most of the cavity excluding this area, however, the temperature gradients are gentle; This indicates the remarkable effects of mechanically-driven circulations. When magnetic field is applied, the effect of driven lid is decreased and temperature gradients are gentler at bottom zone of the cavity. A thermally stratified region in the vertical direction appears in the bulk of the cavity when Hartmann numbers increases to 100. With increasing Grashof number conduction heat transfer plays more effective role and therefore the temperature distribution contour demonstrates that the fluid is vertically stratified in the stagnant zone at the bottom and middle of the cavity. When Grashof number is increased to10^5 the effect of the buoyancy predominates the forced convection effect and conduction-dominated regime with horizontal isotherms is formed in the most of the cavity. In this case, the intensification of magnetic field from 30 to 100 does not have considerable effect on the flow pattern because the flow is stagnant in the bulk of the cavity. Fig. 4 also infers that the addition of nanoparticles is more effective in lower Grashof number and weaker magnetic field.

Fig. 5 shows the variation of horizontal and vertical velocities along the mid-planes of the cavity

for various Gr and Ha numbers for volume fraction of 0.05.

The maximum vertical velocity decreases when the Gerashof number increases owing to dominant conduction mode, and it decreases when the Hartmann number increases owing to resistive force applied by magnetic field. Fig. 5 (right) depicts horizontal velocity is strongly affected by Hartmann number and Grashof number. When Grashof number is increased buoyancy-driven flow is strengthened and therefore, the bulk of cavity becomes stagnant and the horizontal velocity is close to zero in most of the cavity. By applying magnetic field, lid-driven flow is restricted to the top portion of the cavity and therefore the horizontal velocity varies in this area and remains unchanged (close to zero) in the bulk of cavity where the flow is stagnant.

The effects of Hartmann number on horizontal temperature distribution in mid-plane (right) and Nusselt number (left) on top lid of cavity is illustrated in Fig. 6 for $\varphi = 0.05$. From the figure it is evident, the Nusselt number at the top lid begins with a high value at the left end and reduces monotonically to a low value towards the right end.

This shows the strong influence of circulation in the vicinity of the top lid. An increment of Hartmann number decreases Nusselt number, because that the circulation is limited close to top lid and the middle of cavity experiences stagnant flow. Temperature distribution in the middle of the cavity is strongly affected by Hartman number and Grashof number. Since the buoyancy effect is negligible in lower Grashof numbers, much of the temperature variations is achieved in small region near right wall of the cavity. By increasing Hartmann number circulating bubbles, move upward and temperature distribution changes linearly throughout the mid-plane. At higher Grashof numbers, the working fluid is stationary and the resultant temperature distribution attains the linear profile due to main conduction mode. In those ranges of Grashof numbers, magnetic field has smaller effect than that of lower Grashof numbers, as the effect of the magnetic field is negligible for Grashof numbers of 10^5 .

The rate of heat transfer augmentation for nanofluid ($\varphi = 0.05$) rather than clear fluid versus Hartmann number is indicated in Fig. 7. The formulation is as below:

$$E_{\varphi} = \frac{Nu(\varphi = 0.05) - Nu(\varphi = 0)}{Nu(\varphi = 0)} \times 100\% \qquad (23)$$

It is seen from the figure that heat transfer enhances with the addition of nanoparticles and the amount of increment, increases with increasing Grashof number. As the magnetic field effects on the flow, the rate of heat transfer enhancement increases for Grashof numbers of 10^3 and 10^4 and becomes constant in high Hartmann numbers.

Fig.8 illustrates the variation of the average Nusselt number on the top lid of cavity versus of Hartmann number at different Grashof numbers for $= 0.05$. The effect of magnetic field on the overall heat transfer process is clearly depicted in this figure. The average Nusselt number decreases gently with increasing Hartmann number for the dominating forced convection mode (Gr =10^3). Sharper increase of the average Nusselt number with enhancing Hartmann number is seen in Gr=10^5 owing to the suppression forced convective effects and augmentation buoyancy effects.

The effects of nanoparticles on average Nusselt numbers are plotted in Fig. 9 for various Hartmann numbers in Gr=10^5. The increase of the solid concentration increases the effective thermal conductivity and as a result the heat transfer rate. In other words, average Nusselt number enhances with increasing the solid volume fraction. The increase of Hartmann number decreases the heat transfer rate and hence average Nusselt number.

The rate of heat transfer suppression due to magnetic field effect for various Grashof numbers at volume fraction of 0.05 can be seen in Fig. 10. The formulation is as follows:

$$E_{Ha} = \frac{Nu(Ha = 30,100) - Nu(Ha = 0)}{Nu(Ha = 0)} \times 100\% \qquad (24)$$

It is evident from the figure that the magnetic field has unconstructive impact on heat transfer process. In other words, when Hartmann number increases heat transfer suppression increases. For instance at Gr= 10^3 Heat transfer reduction is about 60% for Hartmann number of 30, whereas it is about 70% for Ha=100. The figure also shows increasing in Grashof number weakens the impact of magnetic field.

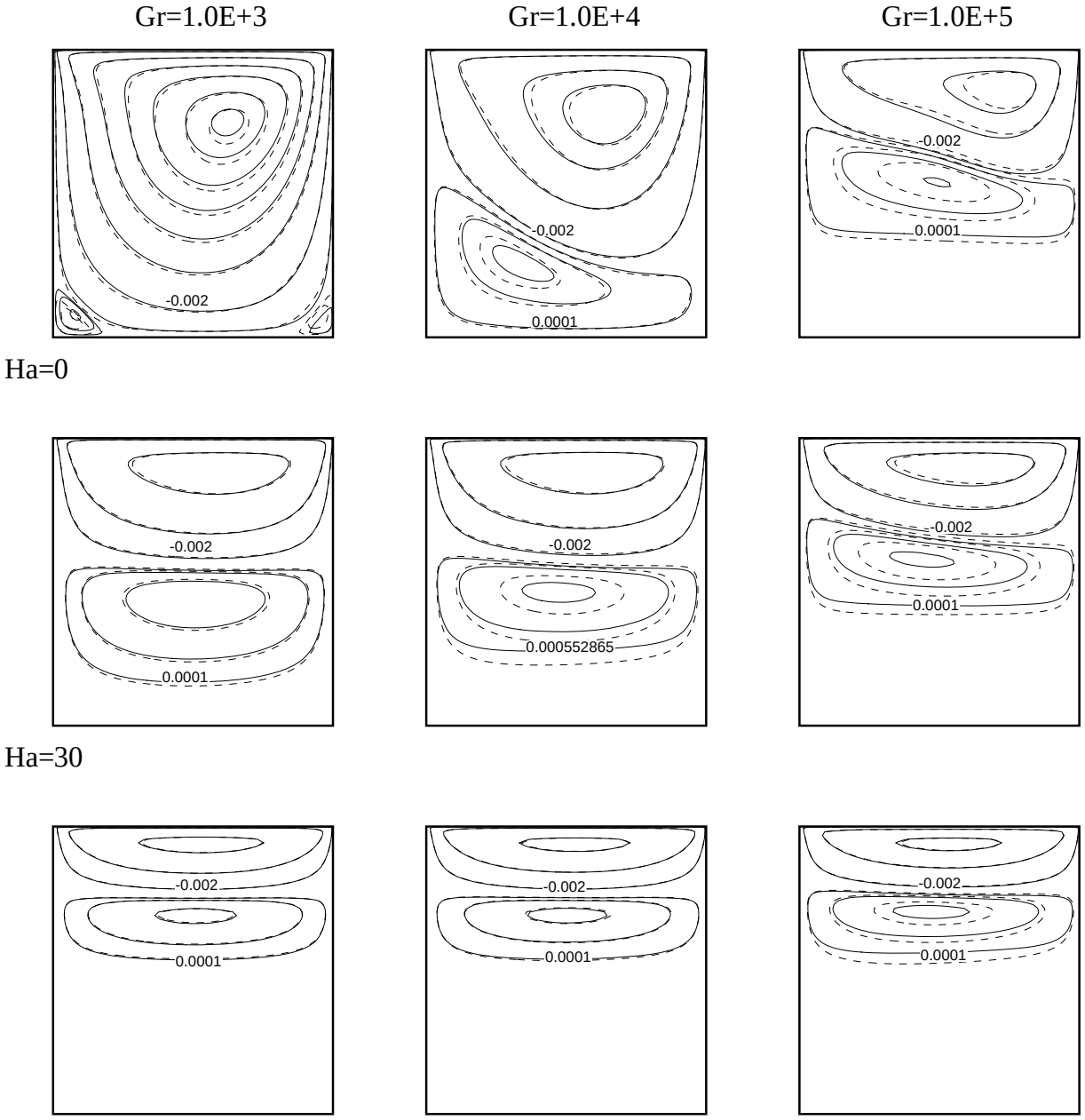

Fig. 3. streamline at various Hartmann number and grashof number (solid line for pure fluid and dashed line for nanofluid with volume fraction of 0.05)

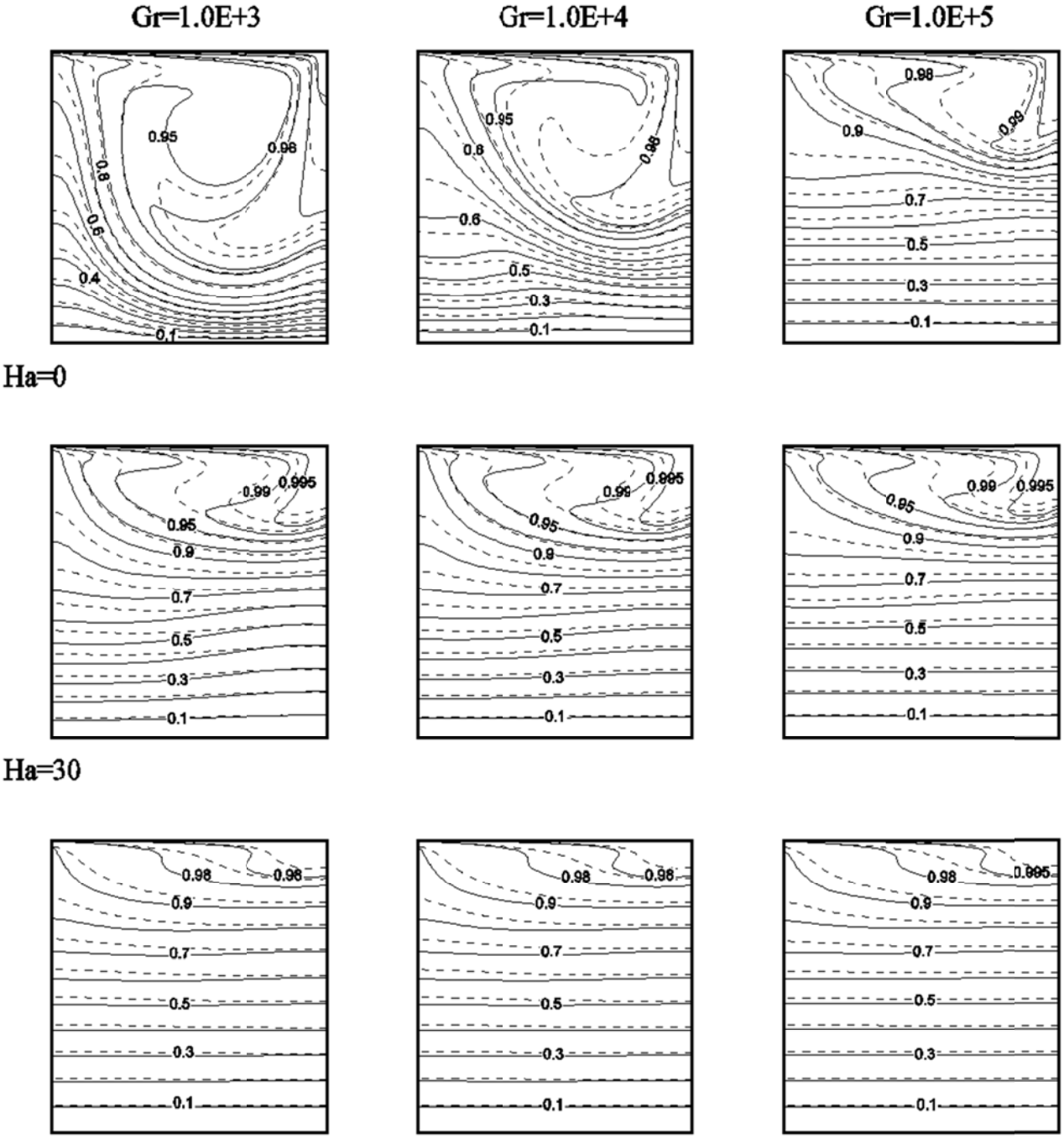

Fig. 4. isotherm at various Hartmann number and grashof number (solid line for pure fluid and dashed line for nanofluid with volume fraction of 0.05)

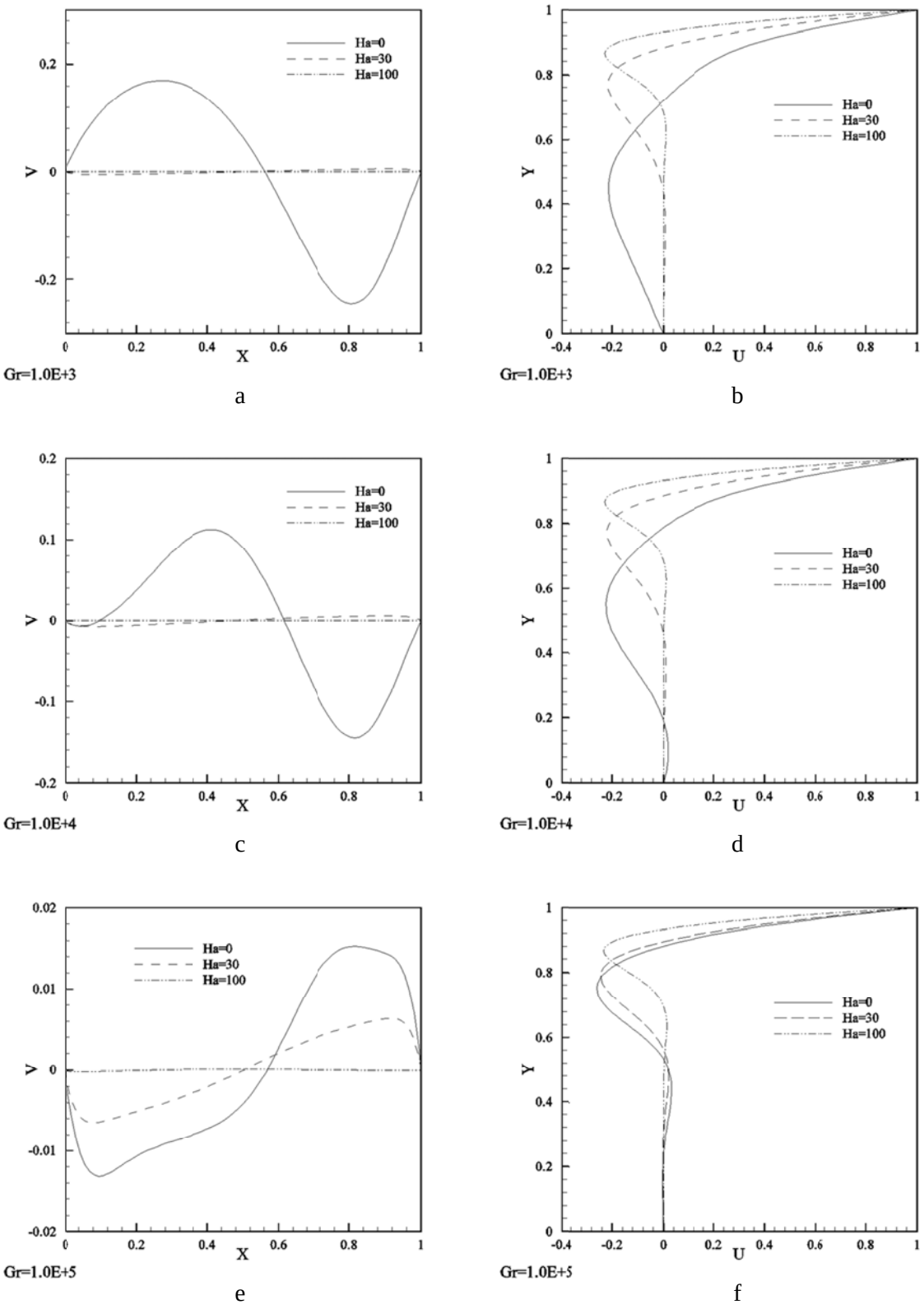

Fig. 5. Variation of u-velocity (left) and v-velocity (right) at the middle of the enclosure for volume fraction of 0.05 at differenct grashof number.

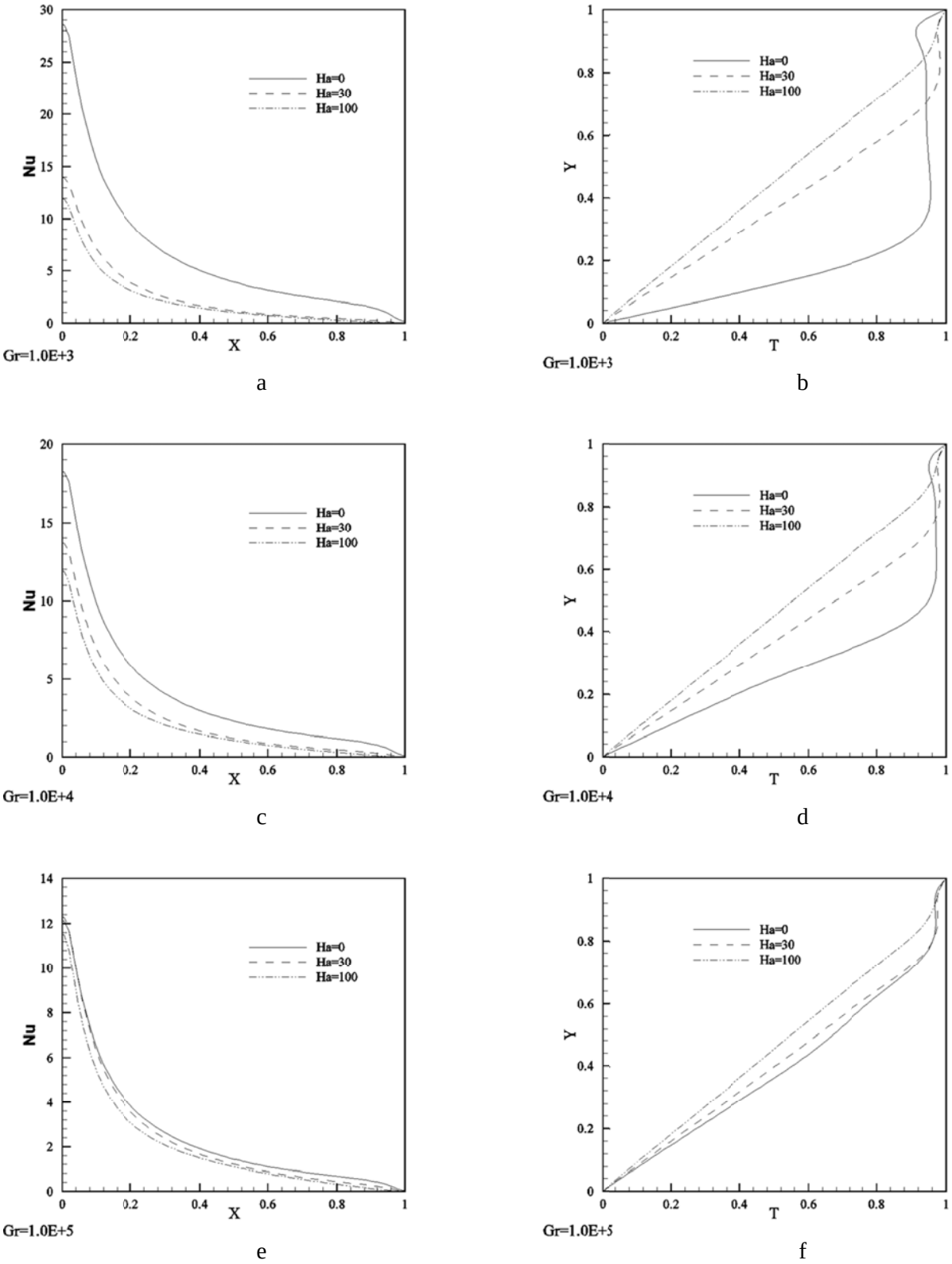

Fig. 6. Local Nussel number at various Hartmann number at the hot surface (right) and temperature profile at the middle of the cavity for different Grashof number at volume fraction of 0.05

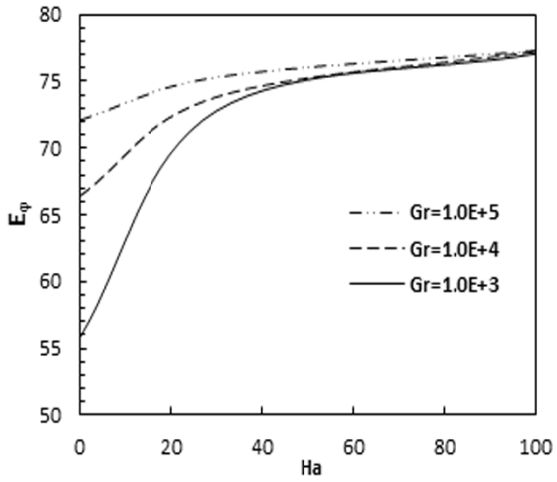

Fig. 7. Ratio of enhancement of heat transfer due to addition of nanoparticles.

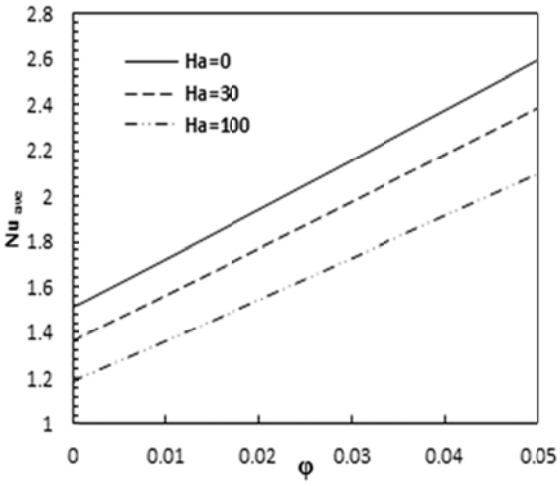

Fig. 9. Variation of the average Nusselt number at the hot surface versus volume fraction number for different Hartmann Grashof number of 105

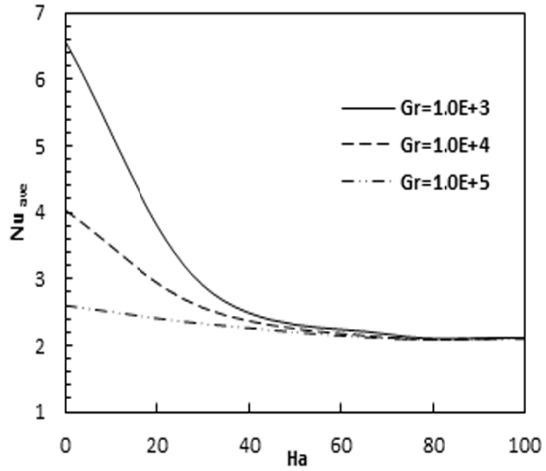

Fig. 8. Variation of the average Nusselt number at the hot surface with Hartmann number for different Grashof number at volume fraction of 0.05

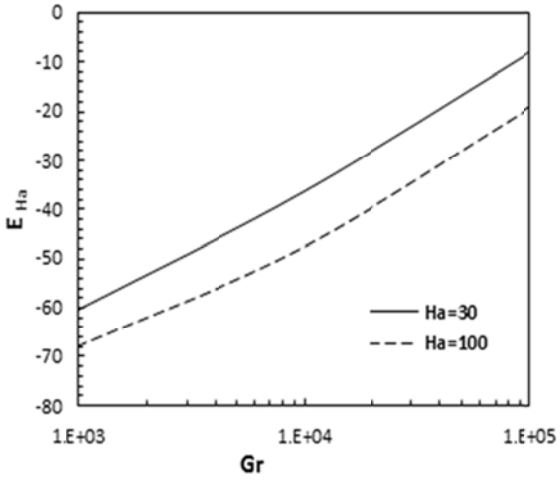

Fig. 10. Ratio of suppression of heat transfer due to magnetic field.

5. Conclusion

Transfer mechanisms. Obtained results released some significant points as follows: The present work studied MHD combined convection in a nanofluid-filled square lid-driven cavity. The governing equations were developed by the SIMLPLE algorithm, which is based on finite volume method. The impact of parameters such as Grashof number, Hartmann number, solid volume fraction was investigated on the fluid flow and heat

1-When Grashof number increases, the effect of driven lid is decreased and buoyancy effect is more dominant at high Grashof numbers. So the main circulation is limited near the top moving wall.

2-Hartmann number decreases the velocity of fluid in the cavity and as a result reduce heat transfer rate and the impact of Hartmann number is more dominant at low Grashof numbers. Figures indicate that the flow is more stagnant at high Hartmann numbers. Figures also illustrates isotherms become vertically stratified when Hartmann numbers increases.

3- Nanoparticles assist the mechanism to have a better heat transfer. In other words, increasing in volume fraction is led to heat transfer amplification, because nanoparticles increase thermal conductivity and augments flow intensity.

References

[1] B. Gebhart, L. Pera**:** The nature of vertical natural convection flows resulting from the combined buoyancy effects of thermal and mass diffusion, Int. J. Heat and Mass Transfer. 14 (1971) 2025-2050.

[2] A. Bejan**:** Mass and heat transfer by natural convection in a cavity, Int. J. Heat Fluid Flow. 6(3) (1985) 2125-2150.

[3] C. Beghein, F. Haghighat, F. Allard: Numerical study of double-diffusive natural convection in a square cavity, Int. J. Heat Mass Transf. 35 (1992) 833-846.

[4] A.J. Chamkha, H. Al-Naser: Hydro magnetic double-diffusive convection in a rectangular enclosure with opposing temperature and concentration gradients, Int. J. Heat Mass Transf. 45 (2002) 2465-2483.

[5] Q.H. Deng, J. Zhou, C.Mei, Y.M. Shen: Fluid, heat and contaminant transport structures of laminar double-diffusive mixed convection in a two-dimensional ventilated enclosure, Int. J. Heat Mass Transf. 47(24) (2004) 5257-5269.

[6] A. M. Al-Amiri, Kh. M. Khanafer, I. Pop: Numerical simulation of combined thermal and mass transport in a square lid-driven cavity, Int. J. Therm. Sci. 46(7) (2007) 662-671.

[7] B. B. Beya, T. Lili: Oscillatory double-diffusive mixed convection in a two-dimensional ventilated enclosure, Int. J. Heat Mass Transf. 50(23-24) (2007) 4540-4553.

[8] M. A. Teamah, W. M. El-Maghlany: Numerical simulation of double-diffusive mixed convective flow in rectangular enclosure with insulated moving lid, Int. J. Therm. Sci. 49(9) (2010) 1625-1638.

[9] F. Talebi, A. H. Mahmoudi, M. Shahi: Numerical study of mixed convection flows in a square lid-driven cavity utilizing nanofluid, Int. Commun. Heat Mass Transf. 37(1) (2010) 79-90.

[10] H. Nemati, M. Farhadi, K. Sedighi, E. Fattahi, A.A.R. Darzi: Lattice Boltzmann simulation of nanofluid in lid-driven cavity, Int. Commun. Heat Mass Transf. 37(10) (2010) 1528-1534.

[11] A. J. Chamkha, E. Abu-Nada: Mixed convection flow in single- and double-lid driven square cavities filled with water-Al_2O_3 nanofluid: Effect of viscosity models, Europ. J. Mech. B/Fluids. Available online 19 March 2012.

[12] F. Talebi, A.H. Mahmoudi, M. Shahi, Numerical study of mixed convection flows in a square lid-driven cavity utilizing nanofluid, International Communications in Heat and Mass Transfer 37 (2010) 79–90.

[13] E. Abu-Nada, A.J. Chamkha, Mixed convection flow in a lid-driven inclined square enclosure filled with a nanofluid, European Journal of Mechanics - B/Fluids (29) (2010) 472-482.

[14] M.A.A. Hamad, I. Pop, A.I. Md Ismail, Magnetic field effects on free convection flow of a nanofluid past a vertical semi-infinite flat plate, Nonlinear Analysis: Real World Applications 12 (2011) 1338–1346.

[15] M.A.A. Hamad, Analytical solution of natural convection flow of a nanofluid over a linearly stretching sheet in the presence of magnetic field, International Communications in Heat and Mass Transfer 38 (2011) 487–492.

[16] B. Ghasemi, S.M. Aminossadati, A. Raisi, Magnetic field effect on natural convection in a

nanofluid-filled square enclosure, International Journal of Thermal Sciences 50 (2011) 1748-1756.

[17] R.C.D. Cruz, J. Reinshagen, R. Oberacker, A.M. Segadaes, M.J. Hoffmann, Electrical Conductivity and stability of concentrated aqueous alumina suspensions, Journal of Colloid and Interface Science 286 (2005) 579–588.

[18] H.C. Brinkman, The viscosity of concentrated suspensions and solutions, The Journal of Chemical Physics 20 (1952) 571–581.

[19] H.E. Patel, T. Pradeep, T. Sundararajan, A. Dasgupta, N. Dasgupta, S.K. Das, A microconvection model for thermal conductivity of nanofluid, pramana- journal of physics 65 (2005) 863–869.

[20] S.V. Patankar, Numerical Heat Transfer and Fluid Flow, Hemisphere Publisher, New York, NY, 1980.

[21] H.K. Versteeg, W. Malalasekera, An introduction to computational fluid dynamics. The finite volume method, John Wiley & Sons Inc, New York, 1995.